Int J Adv Manuf Technol (2009) 40:478–489
DOI 10.1007/s00170-008-1373-0

ORIGINAL ARTICLE

Optimization of pulsed GTA welding process parameters for the welding of AISI 304L stainless steel sheets

P. K. Giridharan · N. Murugan

Received: 24 November 2006 / Accepted: 3 January 2008 / Published online: 9 February 2008

Abstract Optimization of pulsed gas tungsten arc welding (pulsed GTAW) process parameters was carried out to obtain optimum weld bead geometry with full penetration in welding of stainless steel (304L) sheets of 3 mm thickness. Autogenuous welding with square butt joint was employed. Design of experiments based on central composite rotatable design was employed for the development of a mathematical model correlating the important controllable pulsed GTAW process parameters like pulse current (I_p), pulse current duration (T_p), and welding speed (S) with weld bead parameters such as penetration, bead width (W), aspect ratio (AR), and weld bead area of the weld. The developed models were checked for adequacy based on ANOVA analysis and accuracy of prediction by conducting a confirmation test. Weld bead parameters predicted by the models were found to confirm observed values with high accuracy. Using these models, the main and interaction effects of pulsed GTAW process parameters on weld bead parameters were studied and discussed. Optimization of pulsed GTAW process parameters was carried out to obtain optimum bead geometry using the developed models. A quasi-Newton numerical optimization technique was used to solve the optimization problem and the results of the optimization are presented.

P. K. Giridharan (✉)
Department of Mechanical Engineering,
Eswari Engineering College,
Ramawaram,
Chennai, Tamil Nadu 600089, India
e-mail: pkg145@yahoo.co.in

N. Murugan
Department of Mechanical Engineering,
Coimbatore Institute of Technology,
Coimbatore, Tamil Nadu 641 014, India
e-mail: drmurugan@yahoo.com

Keywords Pulsed GTAW process · Welding of stainless steel sheets · Mathematical models · Design of experiments · ANOVA analysis and optimization

1 Introduction

The pulsed GTAW process is suitable for joining thin and medium thickness materials, e.g. stainless steel sheets, and for applications where metallurgical control of the weld metal is critical. With the increased use of mechanized welding, the selection of welding process parameters and welding procedure must be more specific to ensure that the weld bead parameters of good quality are obtained at minimum cost and with high repeatability [1].

In the pulsed GTAW welding process, welding current is pulsed between high and low levels of short or long time interval so that it brings the weld zone to the melting point during the pulse current period and allows the molten weld pool to cool and solidify during the background current period. The weld bead shape will be a series of overlapping weld spots and the amount of overlap depends upon the pulse frequency and welding speed [2]. Pulsed GTAW process parameters are depicted in Fig. 1. Generally, stainless steel welds produced by the pulsed GTAW process have good weld bead geometry in addition to good mechanical and corrosion resistant properties [2]. One of the major problems in welding of thin austenitic stainless steel sheets is variation in penetration from weld-to-weld and heat-to-heat of the base metal. Until now, addition of filler materials has been employed to control the variation in penetration. It is recommended to use stainless steel sheets with sulphur content less than 0.008% for the automated welding process in order to control the variation in weld penetration [2].

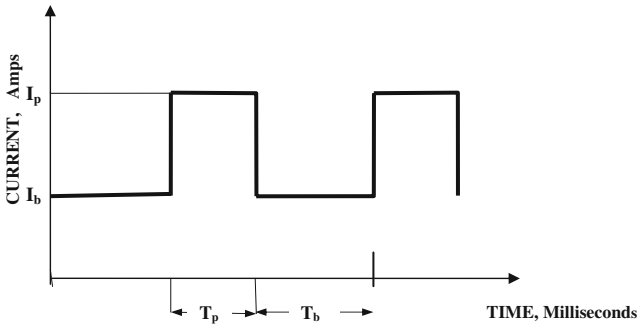

I_b = Base Current, Amps
I_p = Pulse Current, Amps
T_b = Base Current Duration, Milliseconds
T_p = Pulse Current Duration, Milliseconds
$F = 1/(T_p + T_b)$, Pulse Frequency, Hertz

Fig. 1 Pulsed GTAW process parameters

Bead geometry studies using numerical models for conventional welding processes like SAW [1, 3, 4], Co_2 welding [5], GTAW [6, 7], GMAW [8], and FCAW [9], etc. were developed and reported. Very few studies on bead geometry of the pulsed current welding process like pulsed GTAW have been available using sequential experiments or design of experiments employing the Taguchi [6] or modified Taguchi methods [10], and no numerical models correlating pulsed GTAW process parameters with bead parameters like penetration, bead width, bead area, etc. were developed. The main reason that very little has been reported in the pulsed GTAW process, especially using mathematical models, is the difficulty in selecting the optimum combination of pulse parameter for desired weld bead geometry. Hence, most of the recent studies on bead geometry and optimization of the pulsed GTAW process were carried out based on real time control/monitoring using an artificial neural network [11], fuzzy logic [12] and visual image sensing [11, 13–16]. The real-time control methods employed so far in bead geometry studies were of little success, and further research is needed in these approaches.

Selection of optimum pulsed GTAW process parameter combinations to obtain optimum bead parameters using sequential experimentation was reported for welding of thin stainless steel sheets [17, 18]. Application of design of experiments for the study of the effect of the pulsed GTAW process on bead parameters for bead on plate weld (304 type stainless steel) was reported [19]. But a mathematical model correlating pulsed GTAW process parameters with bead geometry to be used to predict the bead parameters was not reported. Moreover, the study was confined to bead on plate weld and not for full penetration weld on thin stainless steel sheets. So from the earlier works, it was observed that some work was carried out to investigate the effect of pulsed GTAW process parameters on stainless steel weld characteristics; but not much effort was made to develop mathematical models to predict the same especially for welding thin stainless steel sheets in a flat position.

Hence, an attempt was made to correlate important pulsed GTAW process parameters to bead geometry of thin stainless steel welds by developing mathematical models. The models developed will be very useful to predict and also to optimize the weld bead parameters or optimizing the pulsed GTAW process parameters for desired bead geometry in a flat position. A statistically designed experiment based on central composite rotatable design was employed for the development of mathematical models [20, 21]. Response surface methodology was used for study of the main and interaction effects of welding process parameters on weld bead parameters [22]. Optimization of welding process parameters was carried out to obtain optimum weld bead geometry using the developed models. In the optimization procedure, the weld bead area model was taken as the objective function (for minimum heat input) along with other weld bead parameter models such as bead width, penetration, and aspect ratio, with their limits as constraints.

2 Experimental procedure

Austenitic stainless steel sheets of type AISI 304L 100×50×3 mm were welded autogenously with square butt joint without edge preparation. The chemical composition of AISI 304L stainless steel sheet is given in Table 1. Experiments were conducted using the pulsed tungsten inert gas welding (TIG) process. Industrial pure and commercial grade argon gases were used for shielding and back purging, respectively. Automatic voltage control available in the welding equipment was used. The voltage and current readings indicated by the equipment were used for heat input calculation. Fixture variation effects were not considered as the same setup was being used throughout the experiment. Some of the welding process parameters were fixed based on earlier work and also from the trial run so as

Table 1 Chemical composition of austenitic stainless steel (304L) sheet

Elements	C	Ni	Cr	Si	Mn	P	S	N	Fe
% by weight	0.017	10.1	18.71	0.22	1.64	0.027	0.047	0.015	69.224

to obtain full penetration weld. The fixed pulsed GTAW process parameters and their values are presented in Table 2.

Independently controllable pulsed GTAW process parameters identified to carry out the experimental work and to develop the mathematical models include: pulse current (I_p), pulse current duration (T_p), and welding speed (S). The ratio between base current and pulse current was maintained at 0.2 throughout the experiments.

Trial runs were conducted to find the limits of each controllable process parameter so as to obtain full penetration weld, free from any visible defects. Because of computational ease and enhanced interpretability of the models, parameters were converted to coded form for developing mathematical models. The upper limit of a factor was coded as +1.682 and the lower limit as −1.682. The coded value for intermediate values was calculated from the relation given by Eq. 1:

$$X_i = (3.364\{(X - X_{\min})/(X_{\max} - X_{\min})\} - 1.682) \quad (1)$$

where X_i is the required coded value of X, X is any value of the variable from $X_{\min}$ to $X_{\max}$, and $X_{\min}$ and $X_{\max}$ are lower and upper limits of the variable X, respectively. The levels determined for process variables with their levels, units, and notations for the pulsed GTAW process are given in Table 3.

A central composite rotatable three factor five level full factorial experimental design consisting of 20 runs was used [23]. Experiments were conducted at random to avoid systematic error creeping into the experimental procedure.

During the trial run, it was observed from the welded plates that penetration was at a minimum between the two pulses, i.e. at the location of maximum bead overlap. Hence, by ensuring full penetration at maximum bead overlap location, full penetration weld can be achieved for the entire length of the weld. So welded plate was cross-sectioned at the location A–A (maximum bead overlap) for the measurement of weld bead parameters and is shown in Fig. 2.

The 10-mm-wide welded specimens were cut and mounted using Bakelite and polished using a standard metallurgical procedure. The electrolytic etching technique using 10% oxalic acid solution was employed for revealing the macrostructure. A photomacrograph of a typical weld specimen cross-sectioned at A–A showing the bead profile at 10× magnification is presented in Fig. 3. Weld bead profiles were traced and bead dimensions such as bead width (W), depth of penetration (P), and weld bead area (BA) were measured by using an optical profile projector and a digital planimeter. Aspect ratio (AR) was calculated from the measured value of bead width and depth of penetration (AR = bead width / depth of penetration).

Heat input is also a very important factor, which affects the bead geometry, mechanical, metallurgical, and corrosion resistant properties of weld. Hence, heat input was also included in the study. The heat input per unit length is proportional to voltage and current as well as inversely proportional to welding speed. In a continuous current GTAW process, heat input is calculated from continuous current, whereas in the pulsed GTAW process, heat input is calculated from the mean current. The equation for mean current [2] is given as:

$$\text{mean current } I_m = \frac{I_p \times T_p + I_b \times T_b}{T_p + T_b} \text{ amps} \quad (2)$$

Heat input (HI) is calculated using Eq. 3 [2]:

$$\text{heat input } HI = \frac{I_m \times V}{S} \times \eta \ (\text{kJ/mm}) \quad (3)$$

I_p pulse current, amps
I_b base current, amps
T_b base current duration, ms
T_p pulse current duration, ms
S welding speed, cm/min
V mean voltage, V
η efficiency of the welding process

For the pulsed GTAW process, arc efficiency is taken as 60% [2]. During the experiment, voltage was found to vary from 13.4 to 14.6 V. Hence, a mean voltage of 14 V is taken for heat input calculation. The observed value of weld bead width, penetration, weld bead area, calculated values of aspect ratio and heat input for pulsed GTA welded specimens along with the design matrix are given in Table 4.

Table 2 Fixed PGTAW process parameters and their values

Sl no.	Process parameters	Values
1	Pulse frequency	1 Hz
2	Arc length	2 mm
3	Mean arc voltage	14 V
3	Tungsten electrode diameter	2.4 mm
4	Electrode vertex angle	60°
5	Gas flow rate (Argon)	
	a. Shielding	10 l/min
	b. Back purging	5 l/min

3 Development of mathematical model

A procedure based on regression was used for the development of mathematical models and to predict the weld bead geometry [8].

The response surface function representing any of the weld bead geometry can be expressed as $Y = f(I_p, T_p, S)$,

Table 3 PGTAW process variables and their levels

Sl. no.	Pulsed GTAW process variables	Notations	Units	Process variable levels				
				−1.628	−1	0	1	1.628
1	Pulse current	I_p	Amps	180	188	200	212	220
2	Pulse current duration	T_p	milliseconds	450	490	550	610	650
3	Welding speed	S	cm / min	11	12.6	15	17.4	19

and the relationship selected is a second-order response surface given as [7]:

$$Y = b_o + b_1 I_p + b_2 T_p + b_3 S + b_{11} I_p^2 + b_{22} T_p^2 + b_{33} S^2 + b_{12} I_p T_p + b_{13} I_p S + b_{23} T_p S \quad (4)$$

where I_p is the pulse current in amps, T_p is the pulse current duration in milliseconds, and S is the welding speed in cm/min. Also, b_0 is a constant term, b_1, b_2, b_3 are coefficients of linear terms, b_{11}, b_{22}, b_{33} are coefficients of second order square terms, and b_{12}, b_{13}, b_{23} are coefficients of second order interaction terms.

Coefficients of the above polynomial equation were calculated by regression as given by Eqs. 5–8 [9]:

$$b_0 = 0.166338\left(\left(\sum X_0 Y\right) + 0.05679\left(\sum\sum X_{ii} Y\right)\right) \quad (5)$$

$$b_i = 0.166338\left(\sum X_i Y\right) \quad (6)$$

$$b_{ii} = 0.0625\left(\left(\sum X_{ii} Y\right) + 0.06889\left(\sum\sum X_{ii} Y\right) - 0.056791\left(\sum\sum X_0 Y\right)\right) \quad (7)$$

$$b_{ij} = 0.125\left(\sum X_{ij} Y\right) \quad (8)$$

where X_i, X_{ii} and X_{ij} are values of first order, second order square, and interaction terms of the process parameters considered for the study. Y is the observed response.

Initial mathematical models were developed using the coefficients obtained from the above equations. Significance of the coefficients was tested using a t test [8] and also by the backward elimination method available in statistical software packages [24]. Final models were developed by using significant coefficients only after eliminating the insignificant coefficient with the associated response without sacrificing much of the accuracy.

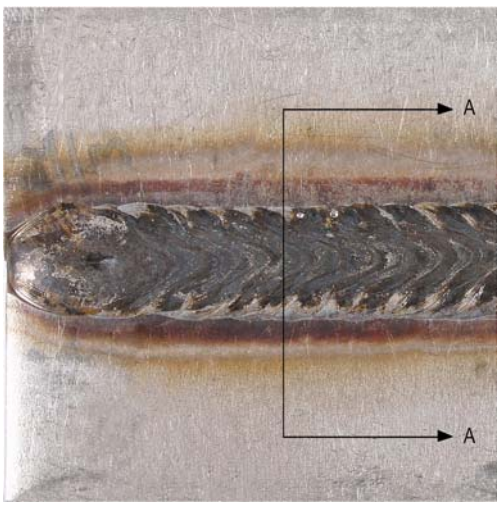

Fig. 2 A typical pulsed GTAW welded specimen (S20) showing the location of cross sectioning (A–A)

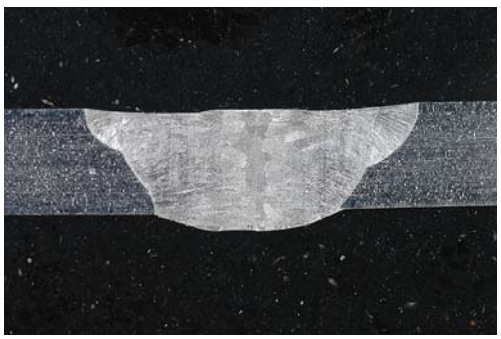

Fig. 3 Photomacrograph of a typical bead profile of a weld specimen (S20) cross-sectioned at A–A (10× magnification)

Table 4 Design matrix and the observed values of bead parameters and heat input

Specimen code	Pulsed GTAW process parameters			Depth of penetration (P) mm	Width (W) mm	Bead area (BA) mm^2	Aspect ratio (AR)	Heat input (HI) kJ/mm
	I_p	T_p	S					
S1	−1	−1	−1	2.36	8.79	12.04	3.725	0.75
S2	1	−1	−1	3.54	9.77	20.93	2.76	0.83
S3	−1	1	−1	3.4	9.24	18.88	2.718	0.87
S4	1	1	−1	3.85	9.8	23.29	2.545	0.97
S5	−1	−1	1	1.66	7.75	7.85	4.668	0.54
S6	1	−1	1	2.98	8.54	13.5	2.866	0.6
S7	−1	1	1	2.37	8.18	10.94	3.451	0.63
S8	1	1	1	3.43	9.33	18.15	2.72	0.70
S9	−1.682	0	0	1.9	7.89	8.62	4.153	0.66
S10	1.682	0	0	3.59	9.52	19.4	2.652	0.78
S11	0	−1.682	0	1.85	7.58	8.68	4.097	0.63
S12	0	1.682	0	3.73	8.79	22.5	2.357	0.81
S13	0	0	−1.682	3.84	10.26	24.66	2.672	0.98
S14	0	0	1.682	1.95	8.385	8.95	4.30	0.57
S15	0	0	0	3.45	9.1	18.44	2.638	0.72
S16	0	0	0	3.78	8.62	20.01	2.28	0.72
S17	0	0	0	3.48	9.14	20.63	2.626	0.72
S18	0	0	0	3.48	9.08	20.91	2.609	0.72
S19	0	0	0	3.84	8.73	21.58	2.273	0.72
S20	0	0	0	3.83	8.75	19.76	2.285	0.72

The developed models were checked for adequacy by regression analysis. The values of adjusted square multiple R and standard error of estimate for both the full and reduced models are given in Table 5. It is evident from the table that the reduced models were better than the full models as reduced models have higher values of adjusted square multiple R and lesser values of standard error of estimate than that of respective full models. The adequacy of developed models was also tested via the analysis of variance technique (ANOVA) [25]. The results of analysis of variance are presented in Table 6. It is evident from Table 6 that all models are adequate.

3.1 Final mathematical model

Final mathematical models with process parameters in coded form as determined by regression analysis are given by Eqs. 9–13:

$$P = 3.637 + 0.502I_p + 0.419T_p - 0.433S - 0.276I_p^2 - 0.265T_p^2 - 0.226S^2 \quad (9)$$

$$W = 8.874 + 0.456I_p + 0.273T_p - 0.509\,S - 0.209T_p^2 + 0.193S^2 \quad (10)$$

Table 5 Comparison of square multiple 'R' values and standard error of estimate for full and reduced models

Bead parameters	Adjusted square multiple R		Standard error of estimate	
	Full model	Reduced model	Full model	Reduced model
Penetration (P)	0.887	0.888	0.262	0.261
Width (W)	0.886	0.904	0.237	0.218
Bead area (BA)	0.899	0.919	1.766	1.583
Aspect ratio (AR)	0.877	0.888	0.264	0.252

Table 6 Results of ANOVA analysis

Bead parameters	First order term		Second order term		Lack of fit		Error term		F ratio	R ratio	Remarks
	SS	DOF	SS	DOF	SS	DOF	SS	DOF			
Penetration (*P*)	8.332	3	2.561	6	0.505	5	0.1829	5	2.76	33.08	Adequate
Width (*W*)	7.103	3	7.396	6	0.303	5	0.2597	5	1.16	18.80	Adequate
Bead area (*BA*)	453.2	3	98.27	6	26.86	5	5.9178	5	4.54	59.77	Adequate
Aspect ratio (*AR*)	6.648	3	3.445	6	0.517	5	0.179	5	2.89	31.32	Adequate

SS sum of squares, *DOF* degree of freedom
Mean sum of squares = sum of square terms / DOF
F ratio = MS of lack of fit / MS of error term
R ratio = MS of first order term & second order term / MS of error terms
F ratio (5, 5, 0.05) = 5.05
R ratio (9, 5, 0.05) = 4.77

$$AR = 2.46 - 0.454I_p - 0.404T_p + 0.344S - 0.284I_p^2 + 0.222T_p^2 + 0.314S^2 + 0.233I_pT_p - 0.174I_pS \quad (11)$$

$$BA = 20.205 + 3.243I_p + 2.942T_p - 3.743S - 2.087I_p^2 - 1.528T_p^2 - 1.099S^2 \quad (12)$$

$$HI = 0.72 + 0.037I_p + 0.055T_p - 0.12S - 0.001I_p^2 - 0.001T_p^2 - 0.019S^2 + 0.004I_pT_p - 0.006I_pS - 0.009T_pS \quad (13)$$

where *P* is the depth of penetration in mm, *W* is the weld bead width in mm, *AR* aspect ratio, *BA* is the weld bead area in mm ^{2}, and *HI* is the heat input in kJ/ mm.

4 Validation of the model

Conformity tests were conducted with the same experimental setup to validate the accuracy of the models. The results of the conformity test are presented in Tables 7 and 8. From the conformity test, it was found that developed models were able to predict the bead parameters with a reasonable accuracy. The validity of the model was tested again by drawing scatter diagrams, which show the degree of closeness between observed and predicted values of weld bead dimensions. A typical scatter diagram for bead area (BA) is shown in Fig. 4.

5 Optimization of bead area (BA)

As the welding process is a multi-objective problem (full penetration, minimum weld bead area, minimum bead width for good quality bead, and maximum welding speed for higher productivity, etc.), the optimum solution is a compromise [26]. The models developed were used for optimization of pulsed GTAW process parameters to obtain optimum weld bead geometry. Bead area is an important weld bead parameter, which in turn controlled by other bead parameters such as penetration, bead width, and aspect ratio. A good control over weld bead area leads to minimum heat input, better control on other bead geometry, and also optimum use of the welding power source.

The limits of constraints were selected based on trial runs. From the trail runs, it was observed that weld bead width less than 9 mm, penetration greater than 3 mm, aspect ratio in the range of 2.5–3, and bead area in the

Table 7 Results of conformity tests—penetration and bead width

Test no.	Process parameter			Penetration (*P*), mm			Bead width (*W*), mm		
	I_p (Amps)	T_p (msec)	S (cm /min)	Predicted values	Observed values	Error %	Predicted values	Observed values	Error %
1	200	550	17	3.11	2.98	−4.27	8.58	8.77	2.19
2	212	603	17.14	3.45	3.31	−4.15	9.11	9.23	1.37
3	211.4	537.65	16.51	3.40	3.28	−3.53	9.00	9.17	1.91
Mean error						−3.98			1.82

$$\text{Error}\% = \frac{\text{ObservedValue} - \text{PredictedValue}}{\text{PredictedValue}} \times 100$$

Table 8 Results of conformity test—aspect ratio and bead area

Test no.	Process parameter			Aspect ratio (*AR*)			Bead area (*BA*), mm^2		
	I_p (A)	T_p (msec)	*S* (cm/min)	Predicted values	Observed values	Error %	Predicted values	Observed values	Error %
1	200	550	17	2.971	2.943	−0.96	16.28	17.051	4.73
2	212	603	17.14	2.721	2.788	2.45	18.51	19.017	2.74
3	211.4	537.6	16.51	2.572	2.795	−2.03	16.63	16.014	−3.7
Mean Error						−0.18			1.25

$$\text{Error}\% = \frac{\text{ObservedValue} - \text{PredictedValue}}{\text{PredictedValue}} \times 100$$

range of 15–20 mm^2 ensured good weld bead geometry with full penetration. So limits of constraints for bead width and bead area were considered less than 9 mm and between 15–20 mm^2, respectively; whereas for aspect ratio and penetration, greater than 2.5 and 3 mm were considered as their respective constraint values.

In the optimization, bead area was taken as the objective function and penetration, bead width, aspect ratio, and bead area with its limits as constraint equations. The optimization problem considered is a nonlinear constrained minimization problem and solved using the quasi-Newton numerical optimization technique [26]. The technique applied is simple, efficient, and also well suited for second order equations [27].

The objective function and constraint equations used for optimization are given as follows.

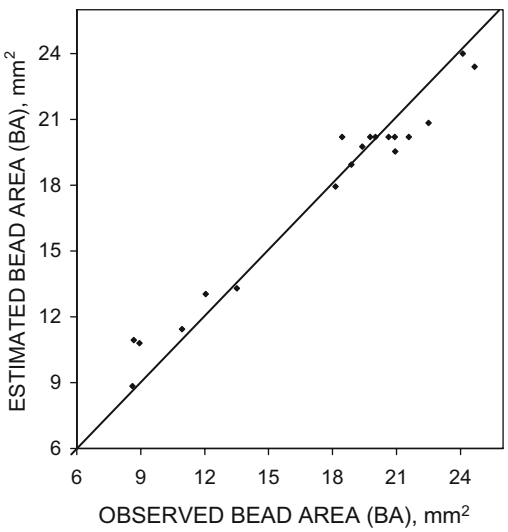

Fig. 4 Scatter diagram for bead area model

5.1 Objective functions

$$\begin{aligned}\text{Minimize } f(x) = {} & 20.205 + 3.243I_p + 2.942T_p \\ & - 3.743S - 2.087I_p^2 - 1.528T_p^2 \\ & - 1.099S^2\end{aligned} \tag{14}$$

which is the bead area in mm ^{2}.

5.2 Constraints equations

The objective function is subjected to the following constraints:

$$P = -\begin{pmatrix} 3.637 + 0.502I_p + 0.419T_p - 0.433S \\ -0.276I_p^2 - 0.265T_p^2 - 0.226S^2 \end{pmatrix} + 3 \tag{15}$$

(penetration and its lower limit),

$$W = \begin{pmatrix} 8.874 + 0.456I_p + 0.273T_p \\ -0.509S - 0.209T_p^2 + 0.193S^2 \end{pmatrix} + 10 \tag{16}$$

(bead width with its upper limit in mm),

$$AR = \begin{pmatrix} 2.46 - 0.454I_p - 0.404T_p + 0.344S - 0.284I_p^2 \\ +0.222T_p^2 + 0.314S^2 + 0.233I_pT_p - 0.174I_pS \end{pmatrix} + 2.5 \tag{17}$$

(aspect ratio with its lower limit in mm),

$$f(x) - 20 \tag{18}$$

(bead area with its upper limit, mm^2),

$$-f(x) + 15 \tag{19}$$

(bead area with its lower limit, mm^2),

$$I_p, T_p, S \leq 1.682 \tag{20}$$

$$I_p, T_p, S \geq -1.682 \tag{21}$$

An optimization tool available in a mathematical processing software package was used for optimization. The software tool "Solver", available in Microsoft Excel 2000, was also used for solving the optimization and was found to confirm the results obtained from the software package. The results of optimization are as follows.

5.3 Optimized pulsed GTAW process parameters

Pulse current	211.4 A
Pulse current duration	537.65 ms
Welding speed	16.51 cm/min

5.4 Optimized bead parameters

Penetration (*P*)	3.4 mm
Bead width (*W*)	9 mm
Aspect ratio (*AR*)	2.57
Bead area (*BA*)	17.89 mm^2

Pulsed GTAW process parameters were set close to the predicted optimum process parameter values and a conformity test was conducted. The results obtained from the conformity test are given in Tables 7 and 8 and found to confirm the predicted results with the observed optimum bead parameters with high accuracy.

6 Results and discussion

Mathematical models were developed correlating important pulsed GTA welding process parameters with the weld bead geometry for welding of thin austenitic stainless steel (304L) sheets.

The possible causes for the main and interaction effects of different pulsed GTAW process parameters on the weld bead parameters were analyzed and are presented graphically in Figs. 5, 6, 7, 8, 9, 10 and 11 for quick analysis and discussed subsequently in Sects. 6.1 and 6.2. The graphs constructed with the help of the developed models (in coded form) provide satisfactory explanations about the effect of the welding process parameters on various bead parameters. Contour and response surface plots were drawn for studying interaction effects using the SYSTAT statistical software package [24] to visualize their nature and are depicted in Figs. 9 and 11.

The effects of heat input on bead parameters were also included in the study using the heat input model, shown in Eq. 13. From the mathematical Eqs. 9, 10, and 12, it is clear that there is no interaction effect of the process parameter

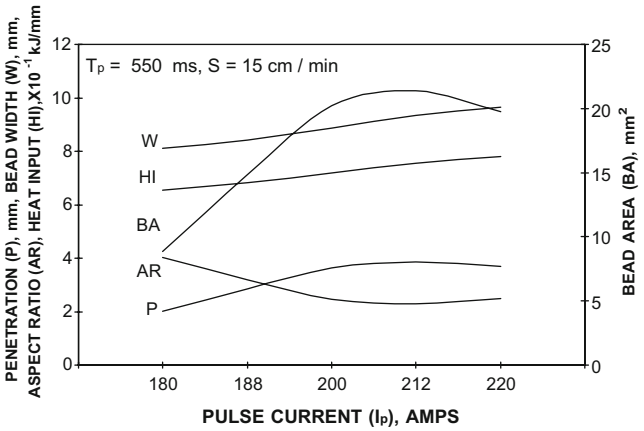

Fig. 5 Direct effect of pulse current (I_p) on bead parameters

on *P*, *W*, and *BA*; whereas from Eq. 11, it is evident that aspect ratio has interaction effects. Hence, an interaction study of process parameters on *AR* alone are studied and discussed subsequently.

6.1 Direct effects

In the study of direct (main) effects of process variable on weld bead parameters, one variable was varied from minimum to maximum level while other variables were kept constant at their middle level. The direct effect of pulsed GTAW process variables on the weld bead parameters and heat input were determined from the models and are discussed below.

6.1.1 Direct effects of pulse current (I_p) on weld bead parameters and heat input (HI)

Figure 5 shows the effect of pulse current (I_p) on penetration (*P*), bead width (*W*), aspect ratio (*AR*), bead area (*BA*), and heat input (*HI*). It is evident from Fig. 5 that as I_p increases from 180 to 220 A, *HI* and *W* increase steadily from 0.65 to 0.78 kJ/mm and 8.1 to 9.6 mm, respectively. Whereas *P*

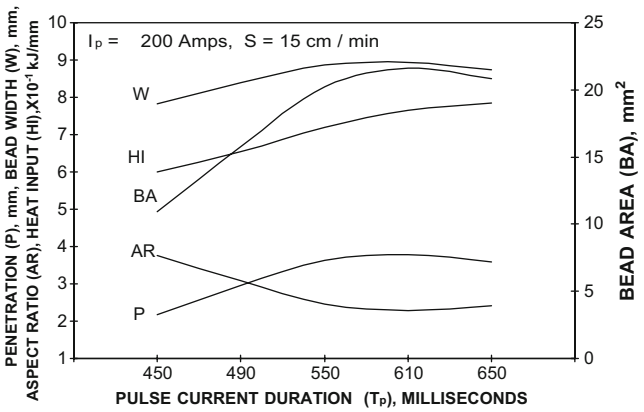

Fig. 6 Direct effect of pulse current duration (T_p) on bead parameters

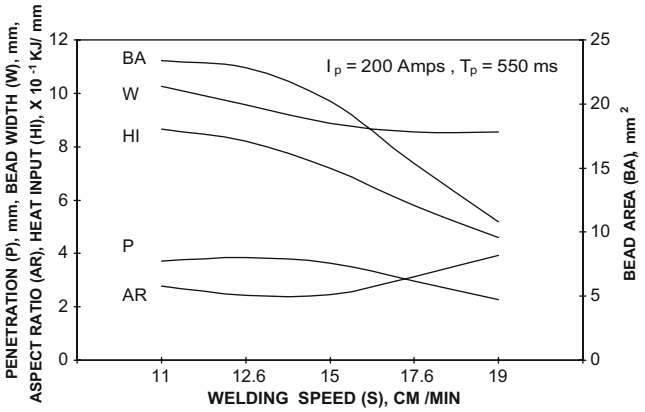

Fig. 7 Direct effect of welding speed (*S*) on bead parameters

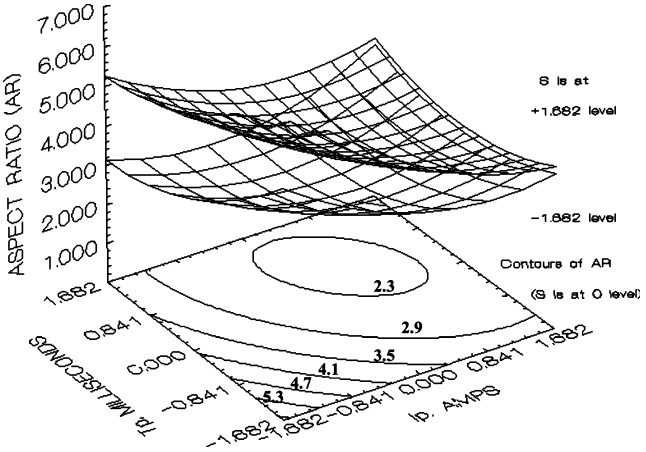

Fig. 9 Response surface and contour plot for interaction effects of pulse current (I_p) and pulse current duration (T_p) on aspect ratio (*AR*)

increases from 2.0 to 3.8 mm as I_p increases from 180 to 212 A, further increase in I_p beyond 212 A brings no significant change in *P*. The initial increase in *P* is due to an increase in *HI*, and reaches maximum at full penetration (when I_p is at 212 A); thereafter is no change in *P* due to dissipation of *HI* along the parent metal, which also may be due to a heat sink effect of the fixture by conduction.

Bead area increases significantly from 8.84 to 21.36 mm^2 as I_p is increased from 180 to 212 A due to increase in *HI*; further increase in I_p beyond 212 A induces only a slight decrease in *BA*. The decrease in *BA* is very small and can be treated as less significant. Initially, increase in *BA* is large due to simultaneous increase in *P* and *W* as I_p is increased from 180 to 212 A. Even though increase in I_p beyond 212 A increases the heat input, it gets dissipated along the base material and also due to heat sink effect of fixture after attaining full penetration. Therefore, less heat input is available for melting the base metal to create appreciable change in *P* and *BA*.

AR initially decreases from 4 to 2.3 as I_p is increased to 212 A because the increase in *P* is larger than that of W, and for further increase in I_p beyond 212 A, the increase in *P* is not significant and hence there is no appreciable change in *AR*. Therefore, it is evident that the effect of increasing pulse current (I_p) has significant influence on all bead parameters up to full penetration and thereafter has very little influence on it. Therefore, I_p is an important process variable affecting bead parameters.

6.1.2 Direct effects of pulse current duration (T_p) on weld bead parameters and heat input (HI)

It is evident from Fig. 6 that as T_p increases from 450 to 650 ms, *HI* increases gradually from 0.59 to 0.78 kJ/mm. *W* and *P* increase considerably from 7.8 to 8.9 mm and 2.2 to 3.8 mm, respectively, as T_p increases from 450 to 550 ms due to increase in *HI*; further increase in T_p beyond 550 ms has very little effect on *W* and *P*. *BA* increases significantly from 10.93 to 21.62 mm^2 as T_p is increased from 450 to 550 ms due to simultaneous increase of *P* and *W* until full penetration; for further increase in T_p beyond 550 A, there are no significant changes in *P* and *W* and hence no significant change in *BA*. The reason for increases in *W*, *P*,

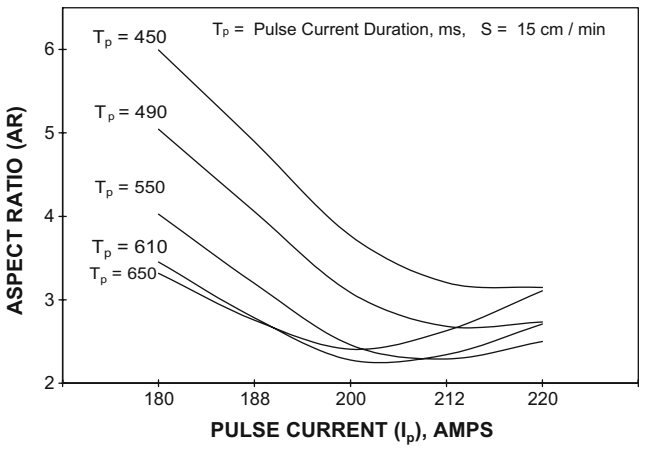

Fig. 8 Interaction effect of pulse current (I_p) and pulse current duration (T_p) on aspect ratio (*AR*)

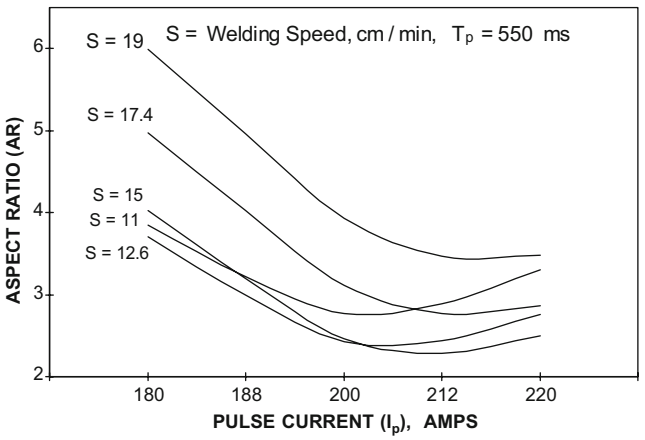

Fig. 10 Interaction effect of pulse current (I_p) and welding speed (*S*)

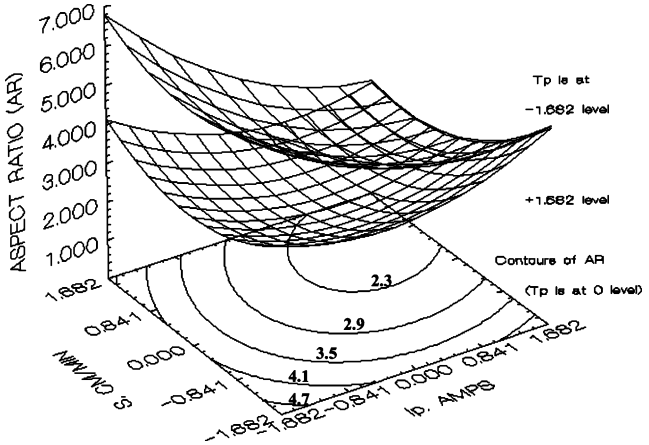

Fig. 11 Response surface and contour plot for interaction effects of pulse current (I_p) and welding speed (S) on aspect ratio (AR)

and BA are due to increase in HI. But after attaining full penetration, increase in HI has no appreciable effect on bead parameters due to dissipation of heat by conduction as explained for I_p in Sect. 6.1.1.

AR initially decreases from 3.7 to 2.3 as T_p increases to 550 ms due to significant increase in P when compared with that of W. There is no appreciable change in AR when T_p is increased beyond 550 ms due to very small changes in P and W indicating a similar trend of I_p on AR shown in Fig. 4. So, it is clear that the effect of increasing pulse current duration (T_p) has significant influence on all bead parameters until full penetration, i.e. at 550 ms; thereafter, increase in T_p has less influence on all bead parameters, showing a similar trend as I_p (Sect. 6.1.1) with less magnitude.

6.1.3 Direct effects of welding speed (S) on weld bead parameters and heat input (HI)

It is apparent from Fig. 7 that as welding speed (S) is increased from 11 to 15 cm/min, HI initially decreases gradually from 0.86 kJ/mm to 0.5 kJ/mm and decreases significantly on further increase in S beyond 15 cm/min. Bead width initially decreases from 10.2 to 8.8 mm and later becomes constant when S is increased beyond 15 cm/min. Moreover, it is apparent that W cannot be reduced below the diameter of the arc zone. So there is no change in W after attaining a certain minimum value. Initially P has very little change when S is reduced to 15 cm/min and then decreases considerably due to large reduction in heat input when S is increased beyond 15 cm/min. BA decreases slowly and then decreases drastically when S is increased beyond 15 cm/min due to significant reduction in P and W.

AR decreases slightly from 2.7 to 2.4 as S is increased to 15 cm/min and then increases significantly to 3.9 as S is increased beyond 15 cm/min. Initial decrease in AR is due to slight increase in P when compared with W as S increased from 11 to 15 cm/min. But significant increase in AR as S is increased beyond 15 cm/min is due to large reduction in P while W remains constant. Therefore, it is clear that as long as S is less than 15 cm/min, bead parameters are less affected, but once S increases beyond 15 cm/min, there is considerable reduction in HI and change in bead parameters. Also, significant reduction in S will result in melting of the base metal at the surface only. Hence, increase in S has high influence on all bead parameters. Thus, S is the most important process variable affecting bead parameters.

Therefore, it is evident from the above discussion (Sects. 6.1.1–6.1.3) on direct effects of process variables on bead parameter that S is the most important and I_p is the next most important influencing process variable, while pulse current duration is the least important among the three process parameters considered for the study.

6.2 Interaction effects

A study on interaction effects of pulsed GTAW process parameters on aspect ratio (AR) of the bead parameter was carried out using the developed AR model. Only two-way interaction effects of the welding process parameters on aspect ratio are discussed below.

6.2.1 Interaction effect of pulse current (I_p) and pulse current duration (T_p) on aspect ratio (AR)

Figure 8 shows the interaction effects of I_p and T_p on AR. It is apparent that as I_p is increased from 180 to 200 A, AR decreases significantly for all values of T_p, whereas further increase in I_p to 220 A, results in little change in AR. The initial decreasing trend of AR may be due to the predominant effect of I_p on AR, and the later slight increasing trend of AR may be due to the predominant effect of T_p on AR. It is also observed that AR is maximum when I_p and T_p are at their minimum level, whereas AR is minimum, when I_p and T_p are at 200 A and 610 ms, respectively, while welding speed is 15 cm/min. As T_p increases from 450 to 490 ms, there is insignificant change to AR, whereas there is considerable increase in AR as T_p is increased from 550 to 650 ms as I_p increases above 200 A. Hence, the effect of increasing T_p has a predominant effect on AR as I_p is increased beyond 200 A.

These effects are also reflected in the response surface and contour plots shown in Fig. 9. The response surface shows that AR increases as S changes from a minimum level to maximum level for all values of I_p and T_p. AR is maximum when I_p and T_p are at their minimum levels and S is at maximum level.

6.2.2 Interaction effect of pulse current (I_p) and welding speed (S) on AR

Figure 10 shows the interaction effect of I_p and S on AR. It is observed that AR is maximum when I_p and S are at their minimum and maximum levels, respectively, whereas AR is minimum when I_p and S are at 212 A and 15 cm/min, respectively. It is apparent that as I_p is increased from 180 to 200 A, AR initially decreases significantly for all values of S. For further increase in I_p beyond 200 A, AR increases considerably as S is decreased from 15 to 11 cm /min, whereas AR becomes more or less steady when S is decreased from 19 to 17.4 cm/min. Hence, it is clear that an increase of I_p from 180 to 200 A has a predominant effect on AR whereas a decrease of S has a predominant effect on AR when I_p is increased from 200 to 220 A.

These effects are also visualized in Fig. 11, which shows the response surface and contour plots for the interaction effects of I_p and S on AR. From the figure, it is evident that AR decreases as T_p is changed from a minimum level to maximum level for all values of I_p and S. AR is maximum when I_p and T_p are at their minimum level and S is at a maximum level.

7 Conclusions

The following conclusions were arrived at from the above investigations:

1. Mathematical models correlating weld bead parameters to pulsed GTAW process parameters were developed for predicting the bead parameters for welding thin stainless steel (304L) sheets of 3 mm thickness with high accuracy.
2. Pulsed GTAW process parameters have shown significant influence on weld bead parameters.
3. Welding speed (S) is the most important and pulse current (I_p) the next most important influencing process variable on bead parameters, while pulse current duration is the least important among the three process parameters considered in this study.
4. Interaction effects of I_p and T_p, and also T_p and S, on AR are significant.
5. Optimum pulsed GTAW process and optimum weld bead parameters for welding of 3 mm thick stainless steel (304L) sheets were found using a quasi-Newton numerical optimization technique. The results were confirmed using conformity tests and found to have good accuracy.

Acknowledgement The authors thank the All India Council of Technical Education and University Grants Commission for providing financial assistance for the project. We also thank Mr. K. R. Ananthanarayanan, Assistant General Manager, Product and Development, Stainless Steel Plant, Steel Authority of India Limited, Salem, India for providing stainless steel sheets for conducting the experiments successfully.

References

1. Murugan N, Parmar RS, Sud SK (1993) Effect of submerged arc process parameters on dilution and bead geometry in single wire surfacing. J Mater Process Technol 37:767–780
2. Cornu J (1988) Advanced welding system, TIG and related processes, vol 3. Springer, Heidelberg, p 61
3. Gunaraj V, Murugan N (2000) Prediction and optimization of weld bead volume for submerged arc process—part 1. Weld J 79 (10):286s–294s
4. Gunaraj V, Murugan N (2000) Prediction and optimization of weld bead volume for submerged arc process—part 2. Weld J 79 (11):294s–331s
5. Kim IS, Son JS, Kim IG, Kim JY, Kim OS (2003) A study on relationship between process variables and bead penetration for robotic CO_2 arc welding. J Mater Process Technol 136(1–3):139–145
6. Tarng YS, Yang WH (1998) Optimization of the weld bead geometry in gas tungsten arc welding by the Taguchi method. Int J Adv Manuf Technol 14(8):549–554
7. Abu Aesh M (2001) Optimization of weld bead dimensions in GTAW of aluminum-magnesium alloy. Mater Manuf Process 16 (5):725–736
8. Murugan N, Parmar RS (1994) Effects of MIG process parameters on the geometry of bead in automatic surfacing of stainless steel. J Mater Process Technol 41:381–398
9. Palani PK, Murugan N (2007) Optimization of weld bead geometry for stainless steel claddings deposited by FCAW. J Mater Process Technol 190(1–3):291–299
10. Balasubramanian M, Jayabalan V, Balasubramanian V (2007) Process optimization of PC TIG welding of Titanium alloy using the modified Taguchi method. Int J Manuf Res 2(4):403–413
11. Chen SB, Zhang Y, Qiu T, Lin T (2003) Robotic welding systems with vision sensing and self-learning neuron control of arc welding dynamic process. J Intell Robot Syst 36(2):191–208
12. Tsai C-H, Hou K-H, Chuang H-T (2006) Fuzzy control of pulsed GTA welds by using real-time root bead image feedback. J Mater Process Technol 176(1–3):158–167
13. Chen SB, Zhang Y, Lin T, Qiu T, Wu L (2004) Welding robotic systems with visual sensing and real-time control of dynamic weld pool during pulsed GTAW. Int J Robot Autom 206(1)2602–2606
14. Chen SB, Zhao DB, Wu L, Lou YJ (2000) Intelligent methodology for sensing, modeling and control of pulsed GTAW, part II—butt welding. Weld J 79(6):164s–174s
15. Chen SB, Zhao DB, Wu L, Lou YJ (2000) Intelligent methodology for sensing, modeling and control of pulsed GTAW, part I—bead-on-plate welding. Weld J 79(6):151s–163s
16. Zhao DB, Yi JQ, Chen SB, Wu L (2004) Surface shape reconstruction of weld pool during pulsed GTAW from its single image, lecture notes in control and information sciences, robotic welding, intelligence and automation, vol 299. Springer, Berlin, pp 56–62
17. Lothongkum G, Chaumbai P, Bhandhubanyong P (1999) TIG pulse welding of 304L austenitic stainless steel in flat, vertical and over head position. J Mater Process Technol 89–90:410–414
18. Lothongkum G, Viyanit E, Bhandhubanyong P (2001) TIG pulse welding parameters of the AISI 316L stainless steel plate at the 6–12h positions. J Mater Process Technol 91–92:312–316

19. Omar AA, Ludin CD (1979) Pulsed plasma—pulsed GTA arc: a study of process variables. Weld J 58(4):97s–105s
20. Hames P, Smith BL (1993) Factorial techniques for weld quality prediction. Met Constr 15:128–130
21. Montgomery DC (2005) Design and analysis of experiments, 6th edn. Wiley, New York
22. Myers RH, Montgomery DC (2002) Response surface methodology, process and product optimization using designed experiments, 2nd edn. Wiley, New York
23. Giridharan PK, Murugan N (2007) Effect of pulsed gas tungsten arc welding process parameters on pitting corrosion resistance of type 304L stainless steel welds. Corros J 63(5):433–441
24. Systat (2004) SYSTAT, version 11. Systat Inc., San Jose, CA
25. Montgomery DC, Peck EA (1992) Introduction to linear regression analysis. Wiley, New York
26. Arora JS (1989) Introduction to optimum design. McGraw Hill, New York
27. Gill PE, Murray W (1981) Practical optimization. Academic, New York